Science Letters ISSN 2345-5463 DOI: https://doi.org/10.47262/SL/9.1.132021002

Research article
2021 | Volume 9 | Issue 1 | Pages 4-11

ARTICLE INFO

Received
October 23, 2020
Revised
January 05, 2021
Accepted
January 06, 2021
Published
February 15, 2021

***Corresponding author**
Oluwatoba E. Oyeneyin
E-mail
emmanueltoba90@gmail.com
oluwatoba.oyeneyin@aaua.edu.ng

Keywords
Density functional theory
Electronic properties
Nonlinear optical properties
Molecular docking
ADMEtox parameters

How to cite
Oyeneyin OE, Adejoro IA, Obadawo BS, Amoko JS, Kayode IO, Akintemi EO, et al. Investigation into the molecular properties of 3-(4-hydroxyphenyl) prop-2-en-1-one 4-phenyl Schiff base and some of its derivatives-DFT and Molecular Docking studies. Sci Lett 2021; 9(1):4-11

Open Access

Investigation into the Molecular Properties of 3-(4-Hydroxyphenyl) Prop-2-en-1-one 4-Phenyl Schiff Base and Some of Its Derivatives-DFT and Molecular Docking Studies

Oluwatoba Emmanuel Oyeneyin[1, 2]*, Isaiah Ajibade Adejoro[3], Babatunde Samuel Obadawo[1], Justinah Solayide Amoko[4], Inyang Olumide Kayode[5], Eric Oluwafisayo Akintemi[6], Nureni Ipinloju[1, 2]

[1] Theoretical and Computational Chemistry Unit; [2] Department of Chemical Sciences, Adekunle Ajasin University, Akungba-Akoko, Ondo State, Nigeria
[3] Department of Chemistry, University of Ibadan, Oyo State, Nigeria
[4] Department of Chemistry, Adeyemi College of Education, Ondo, Ondo State, Nigeria
[5] Phystech School of Biological and Medical Physics, Center for Educational Programs in Bioinformatics, Moscow Institute of Physics and Technology, Dolgoprudny, Russia
[6] Chemistry Unit, Department of Physical Sciences, College of Natural and Applied Sciences, Wesley University, Ondo, Nigeria

Abstract

The structure-property relationship is important in understanding molecular behaviors and their best-fit areas of applications. 3-(4-hydroxyphenyl) prop-2-en-1-one 4-phenyl Schiff base and some of its derivatives were optimized via the density functional theory with Becke three Lee Yang Parr correlation and 6-31G* basis set. The molecular properties calculated were the energies of the frontier molecular orbitals [highest occupied molecular orbital (E_{HOMO}), lowest unoccupied molecular orbital (E_{LUMO}), energy bandgap (E_g), chemical hardness (η), softness (S) and hyperpolarizabilities (β)]. The electronic transitions were calculated with the time-dependent density functional theory methods, the absorption maxima (λ_{abs}), vertical transition energies (ΔE_{ge}), oscillator strengths (*f*) and molecular orbital (MO) components with their percentage contributions were obtained. The anti-microbial efficacy of the molecules was tested against *Staphylococcus aureus* aminopeptidase S (*AmpS*) active site to predict the binding affinities. ADMEtox parameters of all the molecules were also investigated. E_g values ranged from 3.13 to 3.95 eV, β values ranged from 1.45 to 5.81×10^{-30} esu, and their binding affinities ranged from -4.57 to -6.12 kcal/mol, all were

SCAN ME

This work is licensed under the Creative Commons Attribution-Non-Commercial 4.0 International License.

more than that of standard drug, streptomycin (-4.31 kcal/mol). The number of hydrogen bond donors and hydrogen bond acceptors were ranged from 1 to 2 and 3.75 to 5.25, respectively. Variations observed from the calculated molecular properties are the result of varying substituent groups. The molecules can be used as nonlinear optical (NLO) materials and also showed potential for being effective against *Staphylococcus aureus.*

Introduction

To predict the behavior of molecules correctly and ascertain which areas they can best be applied, understanding the relationship between structure and property is very imperative. A lot of work has been reported on how structure influences the properties of molecules [1, 2]. Organic Schiff bases have been investigated and reported for their medicinal applications [3, 4]. Some of them have been applied as nonlinear optical (NLO) materials and served as a protective shield for the human eyes and other sensors from intense laser lights/beams [5, 6] while some have been used to inhibit the corrosion of metals [7, 8]. Energy band gap engineering has been employed by synthetic chemists while designing novel materials with better optoelectronic properties than existing ones. Kroon and coworkers [9] highlighted the contributing factors influencing molecular energy bandgap (E_g) in their work and it has been used as a predictive guide in designing and arriving at materials with optimal applications. The properties of molecules have been predicted via computational techniques in the past and in recent times. Density functional theory (DFT) has been mostly used in predicting the properties of π-conjugated organic molecules [10-13]. Properties like polarizability and hyperpolarizability [14], geometric parameters like bond lengths, bond angles and dihedral angles [11], frontier molecular orbitals (FMOs) energies [15], global reactivity descriptors [16, 17] amongst other properties have been predicted using DFT methods. Molecular docking has also been used to predict the binding affinities of molecules and their mode of action on the receptors of interest [18, 19].

3-(4-hydroxyphenyl) prop-2-en-1-one 4-phenyl Schiff base and some of its derivatives (Fig. 1) were synthesized and reported for their antimicrobial potentials [20]. However, the mode of action of these molecules on the pathogens screened was not ascertained. This study gives an insight into the mode of action or mechanism of its derivatives (ligands) with an enzyme's active site. Also, owing to the nature of the molecules (extensive conjugation), their electronic and NLO properties were investigated for probable applications in optoelectronic and optical limiting devices. This work also predicts the inhibitory action of the molecules against *Staphylococcus aureus* via molecular docking of the molecules (ligands) with *S. aureus* aminopeptidase S (*AmpS*) active sites as described by Odintsov and coworkers [21]. It further investigates optoelectronic and NLO abilities and substituent effects on the molecular properties of the molecules.

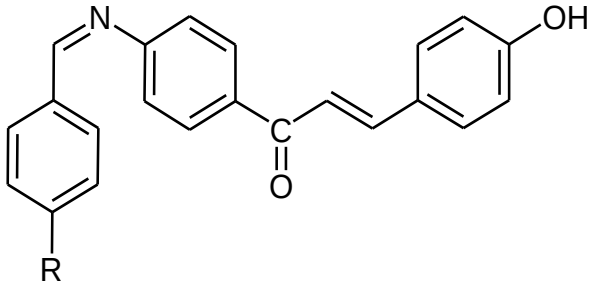

Fig. 1 The structure of the molecule under investigation where R = OH (f) [21]. In this work, the derivatives were uses with substitution at R [(a) R = -H, (b) R = 4-OCH_3, (c) R = -2-OCH_3, 4-OCH_3, (d) R = 4-NO_2, (e) R = 4-Cl, (f) R = 4-OH, (g) R = 3-Cl, 4-Cl.

Methods

Geometry optimization

Quantum mechanics calculations were performed on the modeled molecules, first by conformational search via the molecular mechanics force field (MMFF) method to get the true representatives of the molecules (lowest energy conformer). After that they were subjected to optimization using the DFT method with hybrid Becke Three Lee Yang Parr (B3LYP) correlation [22] and a polar basis set, 6-31G (d) by a restricted hybrid Hartree Fock- DFT (HF-DFT) self-consistent field (SCF) calculation using Pulay DIIS [23] plus geometric direct minimization, all on Spartan 14 computational chemistry software [24]. Frequency calculations were performed to generate the true ground states of the molecules. This level of theory was chosen because it has proven to agree with experimental trends and findings [14, 17]. The calculated

molecular properties included the FMOs energies (energies of the highest occupied molecular orbital, E_{HOMO} and that of the lowest unoccupied molecular orbital, E_{LUMO}), E_g (Eq. 1), hyperpolarizability, β that is a measure of the second harmonic generation (SHG) efficiency and a third-rank tensor described by a 3 × 3 × 3 matrix but became 10 components instead of 27 components due to Kleimann's symmetry (Eq. 2) [25], hardness, η (Eq. 3) and softness, S (Eq. 4) [26]. All these are presented in Table 1.

$$E_g = E_{LUMO} - E_{HOMO} \quad \text{Eq. 1}$$

$$\beta_{eff}\,(\text{x } 10^{-30} \text{ esu}) = [(\beta_{xxx} + \beta_{xyy} + \beta_{xzz})^2 + (\beta_{yyy} + \beta_{yzz} + \beta_{yxx})^2 + (\beta_{zzz} + \beta_{zxx} + \beta_{zyy})^2]^{1/2} \quad \text{Eq. 2}$$

$$\eta = \frac{E_g}{2} \quad \text{Eq. 3}$$

$$S = \frac{1}{\eta} \quad \text{Eq. 4}$$

Molecular docking

Protein preparation

The 3D crystal structure of the human galectin-1 (PDB ID: 1ZJC) was obtained from the protein data bank [27]. *AmpS* has an active site with two metal ions and the protein, 1ZJC was preferred because of its high resolution of 1.8 Å [21]. A protein preparation wizard was used to prepare the downloaded protein by assigning charges and bond orders and deleting water molecules [28]. OPLS3 was used for energy minimization [29].

Ligand preparation

The optimized Schiff base molecules were prepared using Ligprep in Schrödinger Suite 2017-1 with an OPLS3 force field [29]. Epik2.2 in Schrödinger Suite at pH 7.0±2.0 was used to generate the ionization states [30]. The prepared ligands were docked at the active site of 1ZJC after generating receptor grids using OLPS3 force field. XP Ligand docking was performed using Glide of Schrödinger Maestro v 2017-1 [31].

ADMET/Tox screening

The lead compounds were further screened for absorption, distribution, metabolism, excretion and toxicity properties using the QikProp program (https://www.schrodinger.com/qikprop) and Spartan 14 package. These properties are essential in testing drugs for their drug-likeness ability and save cost involved in bioassay studies. Some basic molecular descriptors like molecular weight (M_w), number of hydrogen bond donors (donorHB) and number of hydrogen bond acceptors (acceptHB), etc. were used to ascertain the bioavailability of drugs using Lipinski's rule of five (RO5) [32, 33]. The RO5 states that molecules with M_w<500 have good membrane permeability, also the molecules must possess donorHB <5 and acceptHB <10 [32, 34, 35]. Other properties considered were the total solvent accessible surface area (SASA), which must be between 300.0-1000.0, octanol/water partition coefficient (QPlog Po/w), which must be between -2.0-6.5, value for serum protein binding ($QPlogK_{Hsa}$), which must be between -1.5-1.5 and other descriptors, together with the binding affinities of the molecules (Table 3).

Results and Discussion

Electronic properties

From Table 1, the variation in the E_g values is due to different substituent groups attached as seen in Fig. S1. Unsubstituted (R=H), R= *4*-OCH_3 and R= *4*-OH are almost of similar values while other substituted derivatives are of lower values, with R= *4*-NO_2 being the least. The intramolecular charge transfer (ICT) order is as follows: R = *4*-NO_2 > R= *3*-Cl, *4*-Cl > R= *2*-OCH_3, *4*- OCH_3 > R= *4*-Cl > R= *4*-OCH_3 > R = -H > R= *4*-OH. This is because –NO_2 is the strongest electron-withdrawing group (EWG) among the substituents followed by –Cl and –OCH_3 while OH is an electron-donating group (EDG). A similar trend is observed in their η values since chemical hardness is a direct consequence of energy bandgap (Eq. 3), while the S values follow a reverse

Table 1 Molecular properties of 3-(4-hydroxyphenyl) prop-2-en-1-one 4-phenyl Schiff base and some of its derivatives.

Molecules	E_{LUMO} (eV)	E_{HOMO} (eV)	E_g (eV)	η (eV)	S (eV^{-1})	β ($\times 10^{-30}$ esu)
R= -H	-1.97	-5.90	3.93	1.97	0.509	1.71
R= *4*-OCH_3	-1.82	-5.74	3.92	1.96	0.510	1.59
R= *2*-OCH_3, *4*- OCH_3	-1.72	-5.52	3.80	1.90	0.526	2.09
R= *4*-NO_2	-2.91	-6.04	3.13	1.57	0.639	5.81
R= *4*-Cl	-2.10	-5.94	3.84	1.92	0.521	4.30
R= *4*-OH	-1.85	-5.80	3.95	1.98	0.506	1.45
R= *3*-Cl, *4*-Cl	-2.25	-5.98	3.73	1.87	0.536	4.50

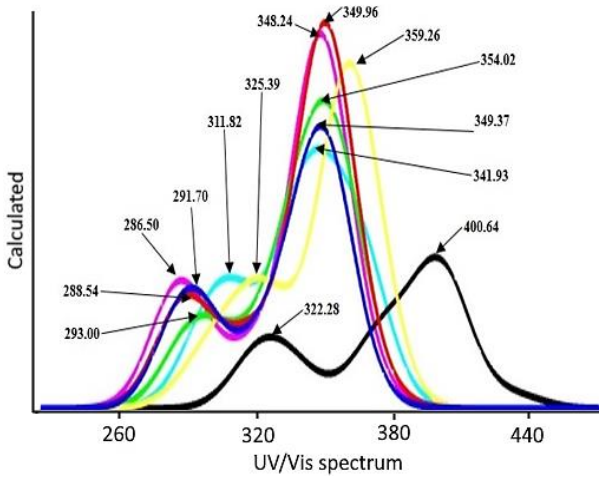

Fig. 2 The UV/Vis spectra of the molecules under investigation.

trend (Eq. 4). Since the two FMOs must overlap in the middle region of the electron density for efficient charge transfer to occur, the ability of the molecules to form polar/multipolar components is influenced by the E_g values, with *4*-NO_2 most likely to possess the highest ability as reported by previous researchers [2, 10]. Hence, there is a need to investigate the variations of E_g values with β values.

Electronic transitions

NLO-active molecules display good absorption and emission properties, the TDDFT calculations were used to obtain the electronic vertical singlet excitation energies. Their absorption maxima (λ_{abs}), oscillator strengths (*f*), excitation energies otherwise known as the vertical transition energies (ΔE_{ge}) and percentage contribution of various configurations to the excitations were obtained and summarized in Table 2 and Fig. 2. These transitions responsible for these absorptions are the π-π* and n-π* transitions. It is noteworthy that R = -H, R = *4*-OCH_3 and R = *4*-OH absorbed around the same region while others (*2*-OCH_3, *4*-OCH_3, *4*-NO_2, *4*-Cl and *3*-Cl,*4*-Cl) bathochromically shifted the λ_{abs} significantly, which is attributed to their lower E_g values. These variations and shifts in the absorption maxima are indicative that they are correlated with the E_g values. *4*-NO_2 has the lowest E_g value and consequently the highest absorption length, it being the best NLO candidate of the studied molecules will be confirmed by its *β* value regarding other analogs.

Nonlinear optical properties

Molecules exhibiting NLO responses display asymmetric polarization brought about by EDGs and EWGs once the system is π-conjugated. As it has been shown earlier that these groups also altered the E_g values of the molecules, it is, therefore, pertinent to look at the *β* values and the relationship with E_g values. It is evident that the –NO_2 substituted analog has the largest NLO response. The order of NLO response is as follows: R = *4*-NO_2 > R= *3*-Cl, *4*-Cl > R= *4*-Cl > R= *2*-OCH_3, *4*-OCH_3 > R = -H > R= *4*-OCH_3 > R= *4*-OH. The NLO responses derived show clearly that the greater the number and the stronger the EWGs, the greater the NLO response. This is because there will be a greater push-pull effect in the molecules as EWGs are added, which consequently results in larger hyperpolarizability values. This correlates with the energy band gap earlier discussed that *β* values increase with the decrease in E_g values (Fig. 3). Therefore, *2*-OCH_3, *4*-OCH_3, *4*-NO_2, *4*-Cl and *3*-Cl,*4*-Cl derivatives are all better and are identified as better choices as NLO materials. However, all the studied molecules have higher *β* values than

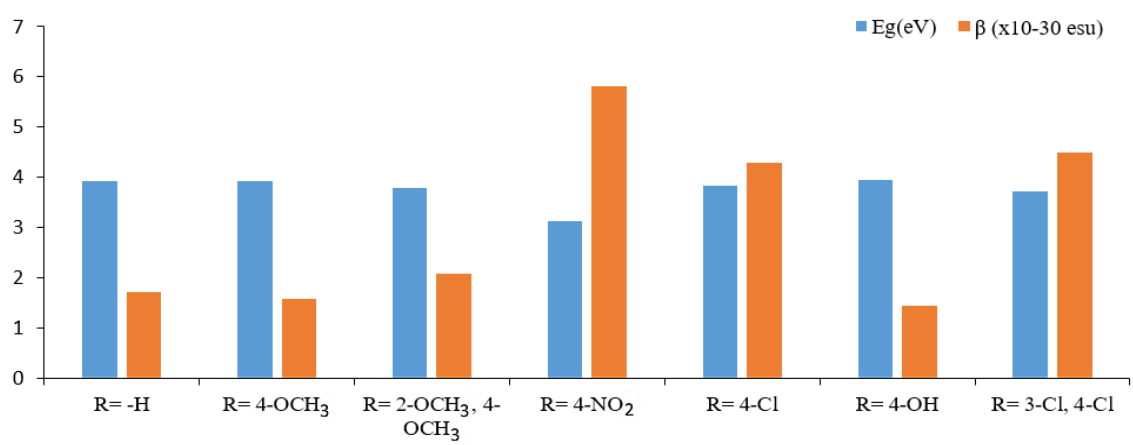

Fig. 3 The relationship/variation of energy bandgap (Eg) with hyperpolarizability (*β*).

Table 2 The absorption maxima (λ_{abs}), vertical transition energies (ΔE_{ge}), oscillator strengths (OS) and molecular orbital (MO) components of 3-(4-hydroxyphenyl) prop-2-en-1-one 4-phenyl Schiff base and some of its derivatives.

Molecules	λ_{abs} (nm)	ΔE_{eg} (eV)	OS (*f*)	MO components and contributions
R= -H	349.37	3.55	0.6632	HOMO -> LUMO 57% HOMO-1 -> LUMO 35%
	291.70	4.25	0.2300	HOMO-3-LUMO 28% HOMO-2-LUMO+1 21%
R= *4*-OCH_3	349.96	3.54	0.9423	HOMO -> LUMO 74%
	288.54	4.30	0.2630	HOMO-3-LUMO 46% HOMO-LUMO+1 17%
R= *2*-OCH_3, *4*- OCH_3	359.26	3.45	0.7376	HOMO -> LUMO 61% HOMO-3 -> LUMO 17% HOMO-1 -> LUMO 12%
	325.30	3.81	0.2030	HOMO-LUMO+1 51% HOMO-2-LUMO 20%
R= *4*-NO_2	400.64	3.09	0.3508	HOMO-1 -> LUMO 85%
	322.28	3.85	0.1453	HOMO-3-LUMO 75%
R= *4*-Cl	354.02	3.50	0.6002	HOMO -> LUMO 73% HOMO-1 -> LUMO 22%
	293.00	4.23	0.1607	HOMO-2-LUMO+1 32% HOMO-LUMO+1 19%
R= *4*-OH	348.24	3.56	0.9173	HOMO -> LUMO 77%
	286.50	4.33	0.2853	HOMO-4-LUMO 71%
R= *3*-Cl, *4*-Cl	341.93	3.63	0.5256	HOMO-1 -> LUMO 47% HOMO-2 -> LUMO 11%
	311.82	3.98	0.1996	HOMO-1-LUMO+1 63% HOMO-2-LUMO 17%

urea (0.65 $\times 10^{-30}$ esu), a standard for organic NLO materials [14]. *4*-NO_2 (5.81 $\times 10^{-30}$ esu) has β values 8.94 times higher than that of urea. All these molecules can be used as NLO devices, with the best of them being *4*-NO_2, R= *4*-Cl, R= *2*-OCH_3, R= *3*-Cl, *4*-Cl and *4*- OCH_3.

Antimicrobial potential/docking score

Molecular docking gives vital information about drug/biomolecular interactions, it also probes into the mechanisms of action of drugs with the receptors to form stable complexes with improved efficacy [36]. The information obtained from the docking process can be used to suggest the binding energy, free energy and stability of complexes. In this study, all the molecules showed lower binding energy compared to the standard drug (streptomycin) as presented in Table 3. From the order of chemical interaction, all the molecules were able to interact with and capture some of the reported amino acid residues (His 381, Asp 383 and Try 355) [21] within the 4Å of *AmpS* active site. R= -H was docked into *AmpS* active site with a docking score of -4.72 kcal/mol as presented in Table 3, and the phenol group of R = -H established hydrogen bond communication with the reported aromatic amino acid Try 355. Arg 31 displayed pi-cation bond to R = -H, which contributes to its stability within the *AmpS* active site as presented in the ligand interaction diagram (Fig. S1). R= *4*-OCH_3 showed the same order of chemical interaction with R = -H but bind higher with -4.57 kcal/mol as presented in Fig. S2 with pi-cation interactions between the phenyl ring and Arg 31, pi-pi stacking with His 381 and hydrogen bonding between the hydroxyl group and Tyr 355. R = *2*-OCH_3 and *4*-OCH_3 showed the same bond communications with above-discussed molecules but for a pi-pi stacking with reported aromatic amino acid residue His 381 with the docking score of -4.59 kcal/mol (Fig. S3). The π-π stacking interaction, an attractive non-covalent interaction, refers specifically to interactions involving aromatic groups containing π bonds. R = *4*-NO_2 showed no hydrogen bond communication with any of the resident amino acid residues, but the nitrobenzene group of R = *4*-NO_2 communicated with the Glu 106 with the strongest non-covalent salt bridge for stabilization in the active site, which was established with the docking score of -5.47 kcal/mol as presented in Fig. S4. R = *4*-Cl showed no communication with the resident amino acid residues but was seen within the 4Å of the enzyme active site with the lowest docking score of -6.12 kcal /mol (Fig. S5). R= *4*-OH

Table 3 ADME and drug-likeness properties of 3-(4-hydroxyphenyl) prop-2-en-1-one 4-phenyl Schiff base and some of its derivatives against *Staphylococcus aureus* aminopeptidase S (*AmpS*) active site.

Molecules	Binding affinity (kcal/mol)	SASA	M_w (amu)	Donor HB	Accpt HB	QPlog Po/w	QPlog HERG	QPlog BB	QPlog Khsa
R= -H	-4.72	662.91	327.38	1	3.75	4.67	-7.47	-1.06	0.61
R= *4*-OCH_3	-4.57	698.23	357.41	1	4.50	4.76	-7.31	-1.14	0.62
R= *2*-OCH_3, *4*- OCH_3	-4.59	737.75	387.44	1	5.25	4.89	-7.24	-1.23	0.64
R= *4*-NO_2	-5.47	703.18	372.38	1	4.75	3.97	-7.41	-2.23	0.57
R= *4*-Cl	-6.12	686.89	361.83	1	3.75	5.16	-7.37	-0.91	0.73
R= *4*-OH	-4.87	675.31	343.38	2	4.50	3.89	-7.34	-1.72	0.41
R= *3*-Cl, *4*-Cl	-4.81	707.43	396.27	1	3.75	5.59	-7.28	-0.78	0.84
Standard drug (Streptomycin)	-4.31	804.54	581.57	16	25.25	-5.93	-5.39	-5.02	-1.90

Where predicted IC_{50} value for blockage of HERG K^+ channels, QPlogHERG = concern below -5; QPlogBB (predicted blood/brain partition coefficient) = -3.0-1.2; HB = hemoglobin; SASA = solvent accessible surface area.

derivative was able to communicate with Tyr 355, Glu 106 and Arg 90 by hydrogen bond and was stabilized by a pi-cation bond with Arg 31with the docking score of -4.87 kcal/mol (Fig. S6). R = *3*-Cl, *4*-Cl molecule phenol group communicated with the reported aromatic amino acid residue with hydrogen bond and stabilized by pi-cation with Arg 31 as presented in Fig. S7. Finally, binding communication of streptomycin (Fig. S8), a well-studied antimicrobial drug for bacteria-derived infection. Streptomycin amide and hydroxyl group donated hydrogen bond to Glu 106, and His 381 and its oxygen group accepted one hydrogen bond from Thr 339 for stabilization at the active site but showed the highest binding energy of -4.31 kcal/mol, thus showed it less affinity for the *Staphylococcus aureus* aminopeptidase S (*AmpS*). It is evident from the study that all the Schiff base molecules exert stronger binding affinities for inhibition of *AmpS* as calculated by the glide scoring function compared to streptomycin. This binding affinity may speak of the anti-microbial efficacy of all the molecules.

ADME analysis

The ADME (absorption, distribution, metabolism, and excretion) properties of all the molecules and streptomycin were evaluated to explain their pharmacokinetic properties and to determine the fitness of molecules as drugs (Table 3). From the results, it was observed that the blood or brain barrier permeability of the standard compound was out of the acceptable range, which is very important for a drug to pass through those barriers. All the molecules under investigation showed QPlogBB value range -2.23-1.00, which is better than streptomycin (-5.020) where the acceptable range is -3.0 to 1.2. The number of hydrogen bond donor and acceptor and the solvent-accessible surface area (SASA) are acceptable. The predicted IC_{50} value for blocking HERG K^+ channel was very close to the acceptable range for streptomycin (-5.390) and those of the molecules were within the normal range. The predicted octanol or water partition coefficient for streptomycin and investigated molecules were also analyzed. The molecules (-2.0-6.5) showed better result than streptomycin (-5.93), where the acceptable range is -2.0 to 6.5. The predicted serum protein binding values of the molecules were within the normal range with the value of 0.57-0.84, but streptomycin was out of the normal range with a value of -1.9. The normal range is -1.5-1.5, thus shows that all the molecules are more likely to reach and bind the *AmpS* active site better than streptomycin to elicit the desired pharmacologic response. It is evident from the ADMETox parameters that all molecules under investigation showed less toxic effect compared to the streptomycin.

Conclusions

The electronic and NLO properties of 3-(4-hydroxyphenyl) prop-2-en-1-one 4-phenyl Schiff base and its derivatives were predicted using the DFT/B3LYP/6-31G*. It was observed that their reactivities and NLO responses were enhanced with different substituent groups. Their NLO responses were compared to that of urea, a standard NLO organic material. The binding affinities and ADMEtox parameters of the molecules were also investigated and compared with those of a standard drug (streptomycin). The results show that all the molecules will reach and bind the *AmpS* active site better than streptomycin to elicit the desired pharmacologic response. It is evident from the ADMETox parameters that all molecules under

investigation showed fewer toxic effects compared to streptomycin. Though our observations here are still subject to confirmatory procedures for pre-clinical and clinical investigations, which best probe the atomistic and pharmacology status of a drug candidate.

Conflict of interest

The authors declare no conflict of interest.

References

[1] Dashti A, Jokar M, Amirkhani F, Mohammadi AH. Quantitative structure property relationship schemes for estimation of autoignition temperatures of organic compounds. J Mol Liq 2019; 300:111797.

[2] Oyeneyin OE, Adejoro IA, Ogunyemi BT, Esan OT. Structural and solvent dependence on the molecular and nonlinear optical properties of 10-octyl thiophene-based phenothiazine and substituted derivatives – a theoretical approach. J Taibah Univ Sci 2018; 2:483–493.

[3] Kulkarni AD. Schiff 's Bases Metal Complexes in Biological Applications. J Anal Pharm Res 2017; 5, no. 1, p. 00127.

[4] Ejelonu BC, Olagboye SA, Oyeneyin OE, Ebiesuwa O A, Bada OE. Synthesis, characterization and antimicrobial activities of sulfadiazine schiff base and phenyl dithiocarbamate mixed ligand metal complexes. Open J Appl Sci 2018; 8:346–354.

[5] Afzal SM, Razvi MAN, Khan SA, Osman OI, Bakry AH, Asiri AM. Physicochemical and nonlinear optical properties of novel environmentally benign heterocyclic azomethine dyes : experimental and theoretical studies. PLoS One 2016; 11:1–25.

[6] Brunel D, Dumur F. Recent advances in organic dyes and fluorophores comprising a 1,2,3-triazole moiety. New J Chem 2020; 44:3546–3561.

[7] Gupta NK, Quraishi MA, Verma C, Mukherjee AK. Green Schiff's bases as corrosion inhibitors for mild steel in 1 M HCl solution: experimental and theoretical approach. RSC Adv 2016; 6:102076–102087.

[8] Kooliyat R, Kakkassery JT, Raphael VP, Cheruvathur SV, Paulson BM. Gravimetric corrosion inhibition investigations of schiff base derived from 5,5-dimethyl-1,3-cyclohexanedione and 2-aminophenol on mild steel in 1 M HCl and 0.5 M H_2SO_4. Int J Electrochem 2019; 1094148:1–13.

[9] Taylor P, Kroon R, Lenes M, Hummelen JC. Small bandgap polymers for organic solar cells (polymer material development in the last 5 years) small bandgap polymers for organic solar cells (polymer material development in the last 5 years). Polym Rev 2008; 48:531–582.

[10] Oyeneyin OE, Ajibade IA, Esan TO. Substituent effects on the structural and nonlinear optical properties of 1-[4-({(E)-[4 (methylsulfanyl)phenyl] methylidene} amino) phenyl] ethanone and some of its substituted derivatives- a theoretical method. Phys Chem Res 2018; 6:667–683.

[11] Adejoro IA, Oyeneyin OE, Adeboye OO, Obaleye JA. Characterization of a novel polymeric zinc (II) complex containing the anti-malarial Quinine as ligand: a theoretical approach (Semi-empirical and DFT methods). Am J Sci Ind Res 2013; 4:111–122.

[12] Semire B, Kolawole A, Odunola OA. Electronic properties' modulation of D–A–A via fluorination of 2-cyano-2-pyran-4-ylidene-acetic acid acceptor unit for efficient DSSCs: DFT-TDDFT approach. Sci African 2020; 7:e00287.

[13] Semire B, Oyebamiji A. Design of (2Z)-2-cyano-2-[2-[(E)-2-[5-[(E)-2-(4-dimethylaminophenyl)vinyl]-2-thienyl]vinyl]pyran-4-ylidene]acetic acid derivatives as D-π-A dye sensitizers in molecular photovoltaics: a density functional theory approach. Res Chem Intermed 2016; 42:4605–4619.

[14] Soma A. Kar T. Experimental and theoretical studies on physicochemical properties of L-leucine nitrate—a probable nonlinear optical material. J Cryst Growth 2012; 356:4–9.

[15] Ogunyemi BT, Oyeneyin OE, Esan OT, Adejoro IA. Computational modelling and characterisation of phosphole adopted in triphenyl amine photosensitisers for solar cell applications. Results Chem 2020; 2: 100069.

[16] Oyeneyin OE, Obadawo BS, Akerele DD, Akintemi EO, Ejelonu BC, Ipinloju N. Experimental and theoretical study on the corrosion inhibitive potentials of Schiff base of aniline and salicyaldehyde on mild steel in 0.5M HCl. Adv J Chem Sect B 2020; 2020:197–208.

[17] Amoko SJ, Akinyele OF, Oyeneyin OE, Olayanju D S, Aboluwoye CO. Experimental and theoretical investigation of corrosion inhibitive potentials of (E)-4-hydroxy-3-[(2,4,6-tribromophenyl) diazenyl] benzaldehyde on mild steel in acidic media. Phys Chem Res 2020; 8:399–416.

[18] Metibemu DS, Oyeneyin OE, Omotoyinbo DE, Adeniran OY, Metibemu AO, Oyewale MB, et al. Molecular docking and quantitative structure activity relationship for the identification of novel phytoinhibitors of matrix metalloproteinase-2. Sci Lett 2020; 8(2):61-68.

[19] Oyebamiji AK, Semire B. Studies of anti-hypertensive activity of 1,4-dihydropyridine derivatives: combinations of dft-qsar and docking approaches. Bull Pharm Res 2016; 6:105–13.

[20] Sawarkar U, Narule M, Chaudhary M. Synthesis of some new 3(4-hydroxyphenyl)prop-2-en-1-one 4-phenyl substituted schiff's bases and their antibacterial activity. Der Pharma Chem 2012; 4:629–632.

[21] Odintsov SG, Sabała I, Bourenkov G, Rybin V, Bochtler M. *Staphylococcus aureus* aminopeptidase S is a founding member of a new peptidase clan. J Biol Chem 2005; 280:27792–27799.

[22] Becke AD. Density-functional thermochemistry. III. The role of exact exchange. J Chem Phys 1993; 98:5648–5652.

[23] Garza AJ, Scuseria GE. Comparison of self-consistent field convergence acceleration techniques. J Chem Phys 2012; 173:54110.

[24] Shao Y, Molnar LF, Jung Y, Kussmann J, Ochsenfeld

C, Brown ST, et al. SPARTAN 14, build 1.01. Irvine (CA); 2014.
[25] Kleinman DA. Nonlinear dielectric polarization in optical media. Phys Rev 1962; 2:1977–1979.
[26] R. G. Pearson, "Absolute electronegativity and hardness correlated with molecular orbital theory," Proc. Natl. Acad. Sci., vol. 83, pp. 8440–8441, 1986.
[27] Lopez-Lucendo MIF, Solis D, Andre S, Hirabayashi J, Kasai K, Kaltner H, et al. Growth-regulatory human galectin-1: crystallographic characterisation of the structural changes induced by single-site mutations and their impact on the thermodynamics of ligand binding. J Mol Biol 2004; 343:957.
28] Sastry GM, Adzhigirey M, Day T, Annabhimoju R, Sherman W. Protein and ligand preparation: parameters, protocols, and influence on virtual screening enrichments. J Comp Aided Mol Des 2013; 27:221–234.
[29] Shivakumar D, Williams J, Wu Y, Damm W, Shelley J, Sherman W. Prediction of absolute solvation free energies using molecular dynamics free energy perturbation and the opls force field. J Chem Theor. Comput 2010; 6:1509–1519.
[30] Shelley JC, Cholleti A, Frye L, Greenwood JR, Timlin MR. Epik: a software program for pK. J Comp Aided Mol Des 2007; 21:681–691.
[31] Friesner RA, Murphy RB, Repasky MP, Frye LL, Greenwood JR, Halgren TA, et al. Extra precision glide: docking and scoring incorporating a model of hydrophobic enclosure for protein-ligand complexes. 2006; J Med Chem 49:6177–6196.
[32] Lipinski CA. Rule of five in 2015 and beyond: target and ligand structural limitations, ligand chemistry structure and drug discovery project decisions. Adv Drug Deliv Rev 2016; 101:34–41.
[33] Lipinski CA. Lombardo F, Dominy BW, Feeney PJ. Experimental and computational approaches to estimate solubility and permeability in drug discovery and development settings. Adv Drug Deliv Rev 2001; 46:3–26.
[34] Lipinski PJ, Lombardo CA, Dominy F, Feeney BW. Experimental and computational approaches to estimate solubility and permeability in drug discovery and development settings. Adv Drug Deliv Rev 1997; 23(1–3):3–25.
[35] Adejoro IA, Waheed SO, Adeboye OO, Akhigbe FU. Molecular docking of the inhibitory activities of triterpenoids of *Lonchocarpus cyanescens* against ulcer. J Biophys Chem 2017; 8(1):1–11.
[36] Rohs R, Bloch I, Sklenar H, Shakked Z, Delbru M. Molecular flexibility in ab initio drug docking to DNA : binding-site and binding-mode transitions in all-atom Monte Carlo simulations. Nucleic Acids Res 2005; 33:7048–7057.